Research Article | Vol. 30, No. 19 / 12 Sep 2022 / Optics Express 34519

Optics EXPRESS

Generation of temporal fading envelope sequences for the FSOC channel based on atmospheric turbulence optical parameters

HAIFENG YAO,[1,3,5] QUN HAO,[1,3,*] CHUNYI CHEN,[3,4] LING LI,[3] YIDI CHANG,[3] SILUN DU,[3] XIANZHU LIU,[3] SHOUFENG TONG,[3] ZHI LIU,[3] SHUQIANG JIA,[2] AND HUILIN JIANG[1,3]

[1] *School of Optics and Photonics, Beijing Institute of Technology,Key Laboratory of Biomimetic Robots and Systems, Ministry of Education, Beijing 100081, China*

[2] *State Key Laboratory of Applied Optics, Changchun Institute of Optics, Fine Mechanics and Physics, Chinese Academy of Sciences, Changchun 130033, China*

[3] *Key Laboratory of Photoelectric Measurement and Control and Optical Information Transfer Technology of Ministry of Education, Changchun University of Science and Technology, 7089 Weixing Road, Changchun 130022, China*

[4] *Chongqing Research Institute, Changchun University of Science and Technology, 618 Liangjiang Avenue, Chongqing 401135, China*

[5] *custfeng@outlook.com*

[*] *qhao@bit.edu.cn*

Abstract: The temporal characteristics of the free space optical communication (FSOC) turbulence fading channel are essential for analyzing the bit error rate (BER) performances and compiling the rationale of adaptive signal processing algorithms. However, the investigation is still limited since the majority of temporal sequence generation fails to combine the autocorrelation function (ACF) of the FSOC system parameters, and using the simplified formula results in the loss of detailed information for turbulence disturbances. In this paper, considering the ACF of engineering measurable atmospheric parameters, we propose a continuous-time FSOC channel fading sequence generation model that obeys the Gamma-Gamma (G-G) probability density function (PDF). First, under the influence of parameters such as transmission distance, optical wavelength, scintillation index, and atmospheric structural constant, the normalized channel fading models of ACF and PSD are established, and the numerical solution of the time-domain Gaussian correlation sequence is derived. Moreover, the light intensity generation model obeying the time-domain correlation with statistical distribution information is derived after employing the rank mapping, taking into account the association between the G-G PDF parameters and the large and small scales turbulence fading channels. Finally, the Monte Carlo numerical method is used to analyze the performances of the ACF, PDF, and PSD parameters, as well as the temporal characteristics of the generated sequence, and the matching relationships between these parameters and theory, under various turbulence intensities, propagation distances, and transverse wind speeds. Numerical results show that the proposed temporal sequence generation model highly restores the disturbance information in different frequency bands for the turbulence fading channels, and the agreement with the theoretical solution is 0.999. This study presents essential numerical simulation methods for analyzing and evaluating the temporal properties of modulated signals. When sophisticated algorithms are used to handle FSOC signals, our proposed temporal sequence model can provide communication signal experimental sample data generating techniques under various FSOC parameters, which is a crucial theoretical basis for evaluating algorithm performances.

#465847
Journal © 2022

https://doi.org/10.1364/OE.465847
Received 2 Jun 2022; revised 7 Aug 2022; accepted 12 Aug 2022; published 7 Sep 2022

Optics EXPRESS

1. Introduction

Free space optical communication (FSOC) offers the advantages of good directionality, enormous bandwidth, high speed, and no electromagnetic interference (EMI). It may be employed as a key technology in the field of 5G and 6G communication [1,2]. The effects of atmospheric turbulence disturbances, which cause light wavefront distortion, light intensity random flicker, and communication signal intersymbol interference (ISI), leading in a deterioration in signal-to-noise ratio (SNR) and bit error rate (BER), are the main hurdle for FSOC. In order to analyze and mitigate the effects of turbulence on different FSOC systems, it is necessary to understand the statistical properties of light intensity fluctuations. Reference [3] shows that the atmospheric turbulence channel fading probability density function (PDF) can more accurately describe the statistical characteristics of light intensity fluctuations. These distribution functions, such as lognormal, exponential, K, Gamma-Gamma (G-G), etc., are frequently employed to depict the distribution characteristics of turbulence channel fading. The communication BER performances are also investigated by combining different communication modulation methods, such as on-off keying (OOK), m-ary pulse amplitude modulation (MPAM), m-ary phase shift keying (MPSK) and multiple quadrature amplitude modulation (MQAM). These PDFs are convincingly verified by numerical simulations and actual field experiments, which portray a process of Gaussian laser beam propagation in statistically uniform and isotropic turbulence fading channel [4–6].

The continuous time variation properties of the atmospheric turbulence fading channel are well known. Under the "Tyler Freeze" assumption, there are reasonable theoretical approximation studies. However, the temporal characteristics are neglected. It prevents the generation of turbulence time-domain continuous signals since the present beam propagation model of light intensity random fluctuation cannot be adequately and accurately defined. Therefore, it is challenging to employ Monte Carlo numerical simulation method to obtain time-continuous signal passing through atmospheric turbulence to process FSOC signal. Usually, when verifying the proposed digital processing algorithm, many FSOC experiments are carried out to sample experimental data in this scenario which need a real field experimental environment or a built equivalent simulation environment in the laboratory [7,8]. However, the experimental equipment used in this method, especially for high-speed FSOC systems, is exceedingly harsh and expensive. Furthermore, it is incomplete because all the turbulence states from strong to weak cannot be traversed.

A continuous Markov process can accurately define this distribution property, according to the PDF analysis of radio frequency (RF) communication fading channel [9,10]. The numerical simulation approach allows for any fading parameter values and non-isotropic fading scenarios. Autoregressive (AR) stochastic models can be employed to compute colored noise and non-Gaussian processes, and autocovariance functions (ACFs) can be employed to generate sequences that fit the temporal characteristics of RF fading channels [11–18]. Stochastic differential equations (SDEs) relying on accurate ACF solutions can also be utilized to describe and estimate its power spectral density (PSD) [10]. The above two methods focus on the PDF analysis of the RF fading channel. Their analytical solutions for PSD and ACF are generally straightforward. However, these functions derivation in turbulence fading channels are a process of solving complex analytical equations because the effects of turbulence disturbances under different scales need to simultaneously be considered. Under certain conditions, atmospheric turbulence ACF can be approximated and simplified to a simple form. Based on Markov models of non-Gaussian exponentially correlated processes, D. Bykhovsky approximated the ACF of turbulence fading channel as a simple exponential form $\exp(-\tau)$ (see [19], Eq. (4); [20], Eqs. (3)–(5)). More than that, he generated a time-domain correlation sequence of lognormal, K, Gamma, and Gamma-Gamma (G-G) by employing stochastic differential equations (SDEs). Assumed that turbulence exists $l_0 \ll \rho \ll \sqrt{\lambda L}$ (l_0, ρ, λ and L denote the inner scale of turbulence, the spatial coherence radius of the optical wave at the receiving point, wavelength, and propagation distance, respectively. A. Jurado et al. deduced ACF into the square form of exponent and then used the Fourier transform to obtain PSD which is the filter function (see [21], Eqs. (5)–(6)). Meanwhile, the AR multi-channel generalization model (see [22], Eq. (8)) was used to solve the temporal sequence under various turbulence. According to the assumptions of Ref. [19], our study team also used the SDEs algorithm to obtain a numerical solution for the Jonson SB_s PDF of the Fiber-FSOC system and employed the real-time sequence to investigate the relationships between system time delay and reciprocity (see [23], Eqs. (15)–(19)).

However, the generation accuracy of the aforementioned temporal sequences is entirely dependent on the ACF approximation, which ignores the high-frequency information of the theoretical values. Despite the existence of a definition for coherence time, it fails to adequately integrate the real FSOC system characteristics (such as propagation distance, light wavelength, scintillation index, atmospheric structure constant, etc.). As a result, the temporal performance of the FSOC fading channel cannot be accurately characterized by calculating these simulation sequences under the engineering measurable parameters for a unified experimental procedure. Therefore, we need to investigate a more accurate method for generating the temporal sequence model of the FSOC fading channel, which can provide an important numerical simulation approach for the analysis of the modulated signal's time-domain characteristics and the BER evaluation. we can provide a signal experimental sample generation technique for advanced FSOC signal processing algorithms under various turbulence fading channel characteristics, and a theoretical basis for algorithm performance evaluation.

In this paper, our purpose is to properly employ the ACF of the atmospheric turbulence channel, which significantly restores turbulence disturbance information at multiple frequency bands, to generate a temporal sequence related to the FSOC parameters without simplifying them. Section 1 is the introduction. a time-domain correlation sequence generation model for turbulence fading channel is given in Section 2. Section 3 indicates the experiments and analysis for temporal sequence generation. Finally, the conclusion is elaborated in Section 4.

2. Time-domain correlation sequence generation model for turbulence fading channel

We begin to consider $B_{\ln X}(\rho)$ large-scale and $B_{\ln Y}(\rho)$ small-scale log-irradiance covariance functions, the ACF model for optical turbulence is given by [24]

$$B_I(\rho) = \exp\left[B_{\ln X}(\rho) + B_{\ln Y}(\rho)\right] - 1, \tag{1}$$

In Ref. [25], complete expressions for $B_{\ln Y}(\rho)$ and $B_{\ln X}(\rho)$ are, respectively,

$$\begin{aligned} B_{\ln X}(\rho) &= 1.06\sigma_R^2 \int_0^1 \int_0^\infty \eta^{-11/6} \exp\left(-\eta/\eta_X\right) J_0(\rho\sqrt{k\eta/L})(1-\cos\eta\xi)d\eta d\xi \\ &\cong 0.16\sigma_R^2 \eta_X^{7/6} {}_1F_1\left(\frac{7}{6}; 1; -\frac{k\rho^2\eta_X}{4L}\right), \end{aligned} \tag{2}$$

$$\begin{aligned} B_{\ln Y}(\rho) &= 1.06\sigma_R^2 \int_0^1 \int_0^\infty (\eta+\eta_Y)^{-11/6} J_0(\rho\sqrt{k\eta/L})(1-\cos\eta\xi)d\eta d\xi \\ &\cong 1.27\sigma_R^2 \left(\frac{k\rho^2}{L\eta_Y}\right)^{5/12} K_{5/6}\left(\sqrt{\frac{k\rho^2\eta_Y}{L}}\right). \end{aligned} \tag{3}$$

where, $\sigma_R^2 = 1.23C_n^2 k^{7/6} L^{11/6}$ is Rytov variance, C_n^2, L, $k = 2\pi/\lambda$ and λ are atmospheric structure constant, propagation distance, number of waves and wavelength, respectively. ${}_1F_1(\cdot)$ and $K_{5/6}(\cdot)$ denote a confluent hypergeometric function and a modified Bessel function of the second

Optics EXPRESS

kind. η_X and η_Y are given by

$$\eta_X = \frac{2.61}{1 + 1.11\sigma_R^{12/5}}, \tag{4}$$

$$\eta_Y = 3\left(1 + 0.69\sigma_R^{12/5}\right). \tag{5}$$

Substitute Eqs. (2)–(5) into Eq. (1), and let $\rho = V_\perp \tau$, we can deduce the ACF of time

$$\begin{aligned} B_I(\tau) =& \exp\left[\frac{0.49\sigma_R^2}{\left(1 + 1.11\sigma_R^{12/5}\right)^{7/6}} {}_1F_1\left(\frac{7}{6}; 1; -\frac{kV_\perp^2\tau^2\eta_X}{4L}\right)\right. \\ &\left. + \frac{0.50\sigma_R^2}{\left(1 + 0.69\sigma_R^{12/5}\right)^{5/6}}\left(\frac{kV_\perp^2\tau^2\eta_Y}{L}\right)^{5/12} K_{5/6}\left(\sqrt{\frac{kV_\perp^2\tau^2\eta_Y}{L}}\right)\right] - 1. \end{aligned} \tag{6}$$

where $V_\perp$ and τ represent transverse wind speed and time index, respectively. We also define normalized ACF by the expression

$$\psi_I(\tau) = \frac{B_I(\tau)}{B_I(0)}. \tag{7}$$

According to the Ref. [26], Eq. (7) is a stationary stochastic process and we can derive its power spectrum form

$$S_I(\Omega) = 4\int_0^\infty \psi_I(\tau)\cos(\Omega\tau)\, d\tau. \tag{8}$$

where, $\Omega = 2\pi\upsilon$, and $\upsilon = 1/\lambda$ denotes light frequency. f_s is sampled to obtain the normalized digital frequency as $\omega = 2\pi/f_s$ in order to further discretize the data. When additive white noise (AWGN) with a power of σ^2 through a transfer function composed of rational filter $H(\omega)$, the temporal signal can be produced [27]. Hence, Eq. (8) can be written as

$$S_I(\omega) = \sum_{n=1}^{\infty} \psi_I(n) e^{-j\omega n} = \left|\frac{B(\omega)}{A(\omega)}\right| \sigma^2 = H(\omega)\sigma^2. \tag{9}$$

where $A(\omega) = 1 + a_1 e^{-j\omega} + \cdots a_n e^{-jn\omega}$, $B(\omega) = 1 + b_1 e^{-j\omega} + \cdots b_m e^{-jm\omega}$. Observing the covariance structure of the autoregressive moving average (ARMA) process [28,29], it can be deduced

$$\begin{cases} \psi_I(0) + \sum\limits_{n=1}^{N} a_i \psi_I(-n) = \sigma^2 \\ \psi_I(m) + \sum\limits_{n=1}^{N} a_n \psi_I(m-n) = 0 \end{cases}, \tag{10}$$

$$\boldsymbol{\Psi}_{I,(n+1)\times(n+1)} \begin{bmatrix} 1 \\ \boldsymbol{\theta}_{n\times 1} \end{bmatrix} = \begin{bmatrix} \boldsymbol{\sigma}^2_{n\times 1} \\ 0 \end{bmatrix} = \begin{bmatrix} \psi_I(0) & \psi_I(-1) & \cdots & \psi_I(-n) \\ \psi_I(1) & \psi_I(0) & & \vdots \\ \vdots & & \ddots & \psi_I(-1) \\ \psi_I(n) & \cdots & & \psi_I(0) \end{bmatrix} \begin{bmatrix} 1 \\ a_1 \\ \vdots \\ a_n \end{bmatrix} = \begin{bmatrix} \sigma^2 \\ 0 \\ \vdots \\ 0 \end{bmatrix}. \tag{11}$$

Optics EXPRESS

where a_i represents the coefficient of the filter, which can be regarded as the transfer function of the turbulence fading channel. Let $\alpha_n = \psi_I(n+1) + \widetilde{\boldsymbol{\Psi}^*_{I,1\times n}}\boldsymbol{\theta}_{n\times 1}$, Eq. (11) can be written as

$$\begin{bmatrix} \boldsymbol{\Psi}_{I,(n+1)\times(n+1)} & & \psi_I(-n-1) \\ & & \boldsymbol{\Psi}_{I,n\times 1} \\ \psi_I(n+1) & \widetilde{\boldsymbol{\Psi}^*_{I,1\times n}} & \psi_I(0) \end{bmatrix} \begin{bmatrix} 1 \\ \boldsymbol{\theta}_{n\times 1} \\ 0 \end{bmatrix} = \begin{bmatrix} \boldsymbol{\sigma}^2_{n\times 1} \\ 0 \\ \alpha_n \end{bmatrix}. \tag{12}$$

Here, $\boldsymbol{\Psi}_{I,n\times 1} = \begin{bmatrix} \psi_I(1) & \cdots & \psi_I(n) \end{bmatrix}^T$, $\widetilde{\boldsymbol{\Psi}_{I,n\times 1}} = \begin{bmatrix} \psi_I{}^*(1) & \cdots & \psi_I{}^*(n) \end{bmatrix}^T$. According to Ref. [30], we employ the Yule-Walker equation to solve Eq. (12) by using the order recursive solution method, we can get

$$\boldsymbol{\theta}_{(n+1)\times 1} = \begin{bmatrix} \boldsymbol{\theta}_n \\ 0 \end{bmatrix} + \xi_{n+1}\begin{bmatrix} \boldsymbol{\theta}_n \\ 1 \end{bmatrix}, \quad \sigma^2(n+1) = \sigma^2(n)\left(1 - |\xi(n+1)|^2\right), \quad \sigma^2(n)\theta(n) = Y(n), \tag{13}$$

$$\sigma^2(n+1) = \sigma^2(n)\left(1 - |\xi(n+1)|^2\right), \tag{14}$$

$$\sigma^2(n)H(\omega) = Y(n). \tag{15}$$

where $\xi(n+1) = -\alpha_n \big/ \sigma^2(n)$. In this way, we can deduce the coefficients $\theta(n)$ of the transfer function of the turbulence fading channel in turn, and can calculate the time-domain correlation sequence Y employing Eqs. (13)–(15). The above is a time-dependent calculation based on AWGN as random values. Still, the PDF is not taken into account, resulting in the generated sequence not obeying the turbulence disturbance theory. For this reason, assuming this system is a free-space receiver and the aperture smoothing effect is not considered, this paper uses the G-G function as the PDF of the turbulence fading channel, its parameters α and β can be related to the turbulence structure constant C_n^2 , which is given by [31]

$$p_I(I) = \frac{2(\alpha\beta)^{(\alpha+\beta)/2}}{\Gamma(\alpha)\Gamma(\beta)I}\left(\frac{I}{\langle I\rangle}\right)^{(\alpha+\beta)/2} K_{\alpha-\beta}\left(2\sqrt{\frac{\alpha\beta I}{\langle I\rangle}}\right), I>0, \tag{16}$$

$$\alpha = \frac{1}{\sigma_X^2} = \frac{1}{\exp(\sigma^2_{\ln X})-1}, \quad \beta = \frac{1}{\sigma_Y^2} = \frac{1}{\exp(\sigma^2_{\ln Y})-1}, \tag{17}$$

$$\sigma^2_{\ln X} = \frac{0.49\sigma_R^2}{\left(1+1.11\sigma_R^{12/5}\right)^{7/6}}, \quad \sigma^2_{\ln Y} = \frac{0.51\sigma_R^2}{\left(1+0.69\sigma_R^{12/5}\right)^{5/6}}. \tag{18}$$

where $\langle I^n\rangle$ represents the n^{th} moment of the light intensity I, $\Gamma(\cdot)$ denotes Gamma function. Note that here I is the theoretical light intensity sequence. When the normalized random light intensity sequence $\left\{\hat{I}_n \big/ \langle I\rangle\right\}_{1\times N}$ obtained from the simulation obeys the Gamma-Gamma PDF, it can be expressed as

$$\left[\hat{I}_1 \big/ \langle\hat{I}\rangle, \hat{I}_2 \big/ \langle\hat{I}\rangle, \ldots \hat{I}_n \big/ \langle\hat{I}\rangle\right]^T = \hat{I} \in PDF_{Gamma-Gamma}, \quad i = 1, 2, \ldots, n \ . \tag{19}$$

According to Ref. [11], $\vec{I}$ is obtained after $\hat{I}$ rearranging in order of Y rank, the correlation coefficient (CC) of the sequence $\rho_{\vec{I},Y}$ can be calculated by

$$\rho_{\vec{I},Y} = \frac{\left\langle\left(\vec{I}(i) - \left\langle\vec{I}\right\rangle\right)(Y(i) - \langle Y\rangle)\right\rangle}{\sqrt{\left\langle\left(\vec{I}(i) - \left\langle\vec{I}\right\rangle\right)^2\right\rangle\left\langle(Y(i) - \langle Y\rangle)^2\right\rangle}} = 1. \tag{20}$$

Therefore, we perfectly map the temporal correlation information of Y to $\vec{I}$ and satisfy

$$\begin{cases} \vec{I} \in PDF_{Gamma-Gamma} \\ \underbrace{\left\langle \left(\vec{I}\,(i) - \left\langle \vec{I} \right\rangle\right) \left(\vec{I}\,(i-m) - \left\langle \vec{I} \right\rangle\right) \right\rangle}_{\vec{\psi}(m)} = \psi_{\vec{I}}\,(m). \end{cases} \tag{21}$$

Equation (21) shows that the $\vec{I}$ generated ACF $\psi_{\vec{I}}\,(m)$ is equal to the numerical simulation result of the theoretical solution Eq. (7) $\psi_I\,(m)$, and the PDF information is preserved. The modeling process of the above Eqs. (1)–(21) can be depicted in Fig. 1. That is, the ACF created is the same as the numerical solution of the theoretical solution (6), and the PDF information is preserved. Figure 1 depicts the modeling method as mentioned above Eqs. (1)–(21).

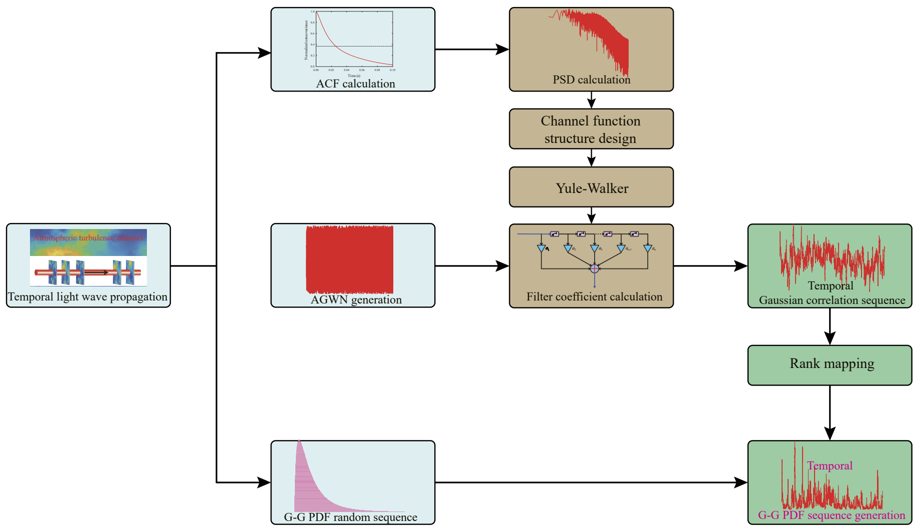

Fig. 1. Implement route for modeling turbulent time-domain correlation signal generation. Where all modeling procedures correspond to Eqs. (1)–(21). The ACF and PSD are determined first, and then the turbulence fading channel function structure is designed using spectral estimation theory. The filter coefficients are calculated utilizing the Yule-Walker algorithm. Moreover, a sequence of temporal Gaussian correlation is generated by combining AWGN. Finally, according to the rank mapping principle of the time-domain Gaussian correlation, the random light intensity sequence obeying the G-G PDF is reordered, which highly restores the turbulence disturbance information in different frequency bands.

3. Experiments and analysis for temporal sequence generation

As shown in Fig. 2, we first investigate the normalized ACF performance under various turbulence intensities, following the implement route of Fig. 1. The blue, black and red lines represent $C_n^2 = 5 \times 10^{-14}$ m$^{-2/3}$, $C_n^2 = 5 \times 10^{-15}$ m$^{-2/3}$ and $C_n^2 = 5 \times 10^{-16}$ m$^{-2/3}$, respectively. The light wavelength, propagation distance and transverse wind speed at this time are given by $\lambda = 1550$ nm, $L = 5000$ m, and $v_\perp = 1$ m/s, respectively. Therefore, the Rytov variances σ_R^2 of turbulence fading channel obtained by our numerical simulation are 19.03, 1.903 and 0.19, respectively, corresponding to the three cases of strong, medium and weak turbulence. The normalized ACF decreases as turbulence intensity increases, and the entire line trend is slanted towards the Y-axis. According to Refs. [23,32], the coherence time τ_d is defined as

$$\psi_I(\tau_d) = e^{-1}. \tag{22}$$

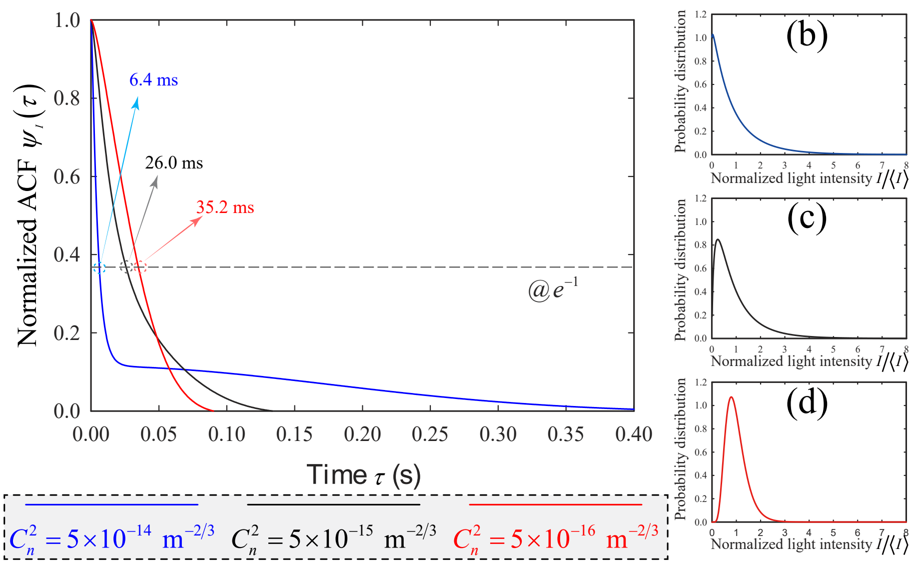

Fig. 2. Normalized ACF and PDF performances for different turbulence fading channels. (a) normalized ACF performances for different turbulence intensities, the blue, black and red lines represent $C_n^2 = 5 \times 10^{-14}$ m$^{-2/3}$, $C_n^2 = 5 \times 10^{-15}$ m$^{-2/3}$ and $C_n^2 = 5 \times 10^{-16}$ m$^{-2/3}$, respectively. The coherence times τ_d are 6.4 ms, 26.0 ms and 35.2 ms, respectively. When ACF tends to 0, i.e., $\psi_I(\tau) \to 0$, the blue, black and red lines denote $\tau_d = 0.3616$ s, $\tau_d = 0.1181$ s and $\tau_d = 0.0821$ s, respectively. The parameters of corresponding normalized light intensity G-G PDF are (b) $\alpha = 7.2306$, $\beta = 1.0453$,(c) $\alpha = 3.9935$, $\beta = 1.7438$ and (d) $\alpha = 12.1495$, $\beta = 10.6132$, respectively. The light wavelength, propagation distance and transverse wind speed at this time are given by $\lambda = 1550$ nm, $L = 5000$ m, and $v_\perp = 1$ m/s, respectively.

After statistical calculation, we can see that the coherence times τ_d corresponding to strong, medium and weak turbulence are 6.4 ms, 26 ms and 35.2 ms, respectively. The coherence time τ_d becomes smaller as turbulence intensity increases, which is demonstrated in Fig. 2(a). Equations (16)–(18) of the aforesaid atmospheric parameters are numerically analyzed for further studying the distribution performance of normalized light intensity at this period. Its form is skewed from exponential to "bell-shaped," and the normalized light intensity distribution is more concentrated, indicating that the scintillation variance is lesser at this time, as illustrated in Figs. 2(b)–2(d), The light intensity scintillation effect mainly consists of large-scale and small-scale scintillation when the turbulence intensity is moderate to weak. The large-scale logarithmic scintillation index tends to zero as turbulence intensity increases, i.e., $\sigma^2_{\ln x} \to 0$, while the small-scale turbulence logarithmic scintillation index tends to be saturated, i.e., $\sigma^2_{\ln y} \to 0.69$. The small-scale is mostly affecting the turbulence disturbance, see Eq. (18), which is one of the reasons for using the G-G PDF as turbulence fading channel function in this paper.

According to Eq. (6), the transverse wind speed $v_\perp$ is another important element impacting the coherence time τ_d, as it can invoke atmospheric movement and trigger random turbulence medium fluctuations on the light wave propagation path. Therefore, the coherence time τ_d performances under various wind speeds $v_\perp$, and propagation distances L and atmospheric turbulence structure constants C_n^2 are depicted in Fig. 3(a). For the convenience of plotting, the turbulence state at this

Optics EXPRESS

time is set to medium $C_n^2 = 5 \times 10^{-15}$ m$^{-2/3}$. When the wind speed $v_\perp$ remains constant, the coherence time τ_d increases as the propagation distance L grows. This is because the coherence time τ_d is a function of $1/L$, indicating that the random medium can be comparable to a sizeable random function in the airspace as the propagation distance L rises. The higher correlation between their media and the longer distance, which reflects the more substantial blocking effect in the time-domain and the larger system robustness, that is, with the increase of distance, the optical time variation characteristics of the entire system weaken, as plotted in Fig. 3(b). However, when the propagation distance L is constant, the coherence time τ_d decreases as the wind speed $v_\perp$ increases. The wind speed accelerates the unpredictability of the turbulence random phase and diminishes spatial coherence under the "Taylor freeze" assumption, resulting in a drop in coherence time, as illustrated in Fig. 3(c).

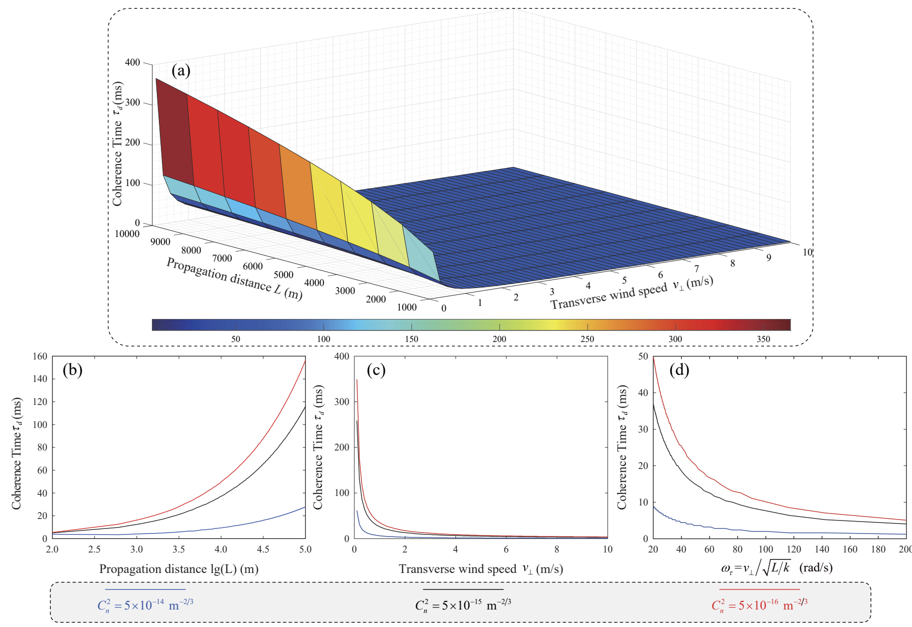

Fig. 3. Contributions of transverse wind speed $v_\perp$ and light wave propagation distance L for the coherence time τ_d of atmospheric turbulence fading channel. (a) Coherence time τ_d distribution performances of atmospheric turbulence fading channel under different transverse wind speeds $v_\perp$ and light wave propagation distances L, the turbulence state at this time is set to medium $C_n^2 = 5 \times 10^{-15}$ m$^{-2/3}$; (b) the relationships between light wave propagation distance L and coherence time τ_d when the transverse wind speed $v_\perp$ = 1m/s; (c) the relationships between transverse wind speed $v_\perp$ and coherence time τ_d when the propagation distance L = 5000 m; (d) the relationships between Fresnel frequency $\omega_\tau = v_\perp/\sqrt{L/k}$ and coherence time τ_d. The blue, black and red lines represent $C_n^2 = 5 \times 10^{-14}$ m$^{-2/3}$, $C_n^2 = 5 \times 10^{-15}$ m$^{-2/3}$ and $C_n^2 = 5 \times 10^{-16}$ m$^{-2/3}$, respectively. The light wavelength is set to λ = 1550 nm.

We define Fresnel frequency to better assess the effect of factors on temporal correlation [33].

$$\omega_\tau = \frac{v_\perp}{\sqrt{L/k}}. \tag{23}$$

Equation (23) takes into account the effects of wind speed, propagation distance and light wavelength, as shown in Fig. 3(d). The coherence time reduces from 25.1331 ms to 18.2480 ms when $\omega_\perp$ = 40 rad/s and the turbulence intensity increases from $C_n^2 = 5 \times 10^{-16}$ m$^{-2/3}$ to

$C_n^2 = 5 \times 10^{-15}$ m$^{-2/3}$. The coherence time at this moment drops to 4.4143 ms if the turbulence level is further enhanced to $C_n^2 = 5 \times 10^{-14}$ m$^{-2/3}$. Because large-scale turbulence clusters lose energy and become small-scale turbulence clusters when the turbulence intensity rises. The diffraction effect of light increases at this time, increasing the phase randomness of the medium of the light wave propagation route, destroying the light wavefront, and shortening the coherence time. As the Fresnel frequency increases further, the coherence time approaches zero.

The atmospheric characteristics of Eq. (6) can be precisely represented, allowing us to construct turbulence fading channel random signals that directly mirror the real turbulence state, as observed in Fig. 3. Therefore, combining Eqs. (1)–(21), the light wavelength λ, transverse wind speed $v_\perp$ and transverse wind speeds $v_\perp$ are set to $\lambda = 1550$ nm, $v_\perp = 1$ m/s and $L = 5000$ m, respectively. Atmospheric turbulence state are also given by $C_n^2 = 5 \times 10^{-14}$ m$^{-2/3}$, $C_n^2 = 5 \times 10^{-15}$ m$^{-2/3}$ and $C_n^2 = 5 \times 10^{-16}$ m$^{-2/3}$, respectively. These parameters are easily measured directly in the actual FSOC system. We can simulate and create time-domain correlated continuous sequence signals in the different turbulent fading channels using the Monte Carlo approach, as illustrated in Figs. 4(a)–4(c). According to Ref. [24] (see Chapt. 8, Eq. (9)), the scintillation index can be expressed as

$$\sigma_{\vec{I}}^2 = \left(\left\langle \vec{I}^2 \right\rangle - \left\langle \vec{I} \right\rangle^2\right) \Big/ \left\langle \vec{I} \right\rangle^2. \tag{24}$$

Despite the insufficient sampling interval and generated data capacity, the scintillation index of Figs. 4(a)–4(c) can be approximated by 1.2210, 0.9667, and 0.1839, respectively. It reveals that with the increase of the turbulence degree, the temporal signal jitter degree increases, and the random fluctuation trend increases. These signals are all time continuity, and the signal envelopes are highly similar to the previous experiments done by our research team (see Ref. [23]).

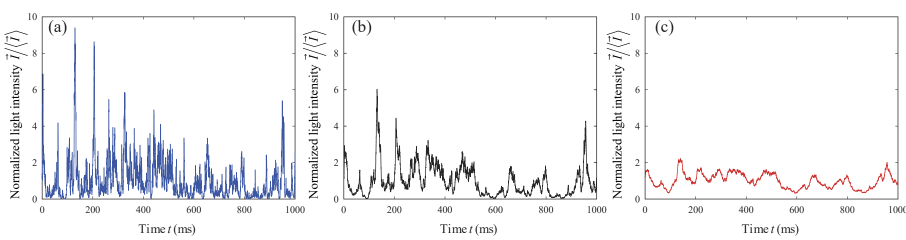

Fig. 4. Generation of time-domain correlated continuous sequence signals in different turbulence fading channel. (a) blue, (b) black and (c) red lines represent $C_n^2 = 5{\times}10^{-14}$ m$^{-2/3}$, $C_n^2 = 5 \times 10^{-15}$ m$^{-2/3}$ and $C_n^2 = 5 \times 10^{-16}$ m$^{-2/3}$, respectively. The light wavelength λ, transverse wind speed $v_\perp$ and propagation distance L are set to $\lambda = 1550$ nm, $v_\perp = 1$ m/s and $L = 5000$ m.

Moreover, we know that Eq. (24) is the scintillation index obtained by engineering calculation, which is mainly composed of the refraction of large-scale turbulence and the diffraction of small-scale turbulence. It can be written as

$$\sigma_I^2 = \exp\left[\frac{0.49\sigma_R^2}{\left(1 + 1.11\sigma_R^{12/5}\right)^{7/6}} + \frac{0.51\sigma_R^2}{\left(1 + 0.69\sigma_R^{12/5}\right)^{5/6}}\right] - 1, \quad 0 \le \sigma_R^2 < \infty. \tag{25}$$

The theoretical scintillation indices of Figs. 4(a)–4(c) can be obtained using theoretical numerical computation, and they are 1.2273, 0.9675, and 0.1843, respectively. Meanwhile, we found that the data deviations are 0.005, 0.0008, 0.006, respectively, all of which are lower than 0.006, manifesting that for different turbulence fading channels, the generation mode of time-domain correlated continuous sequence signal conforms to the theoretical calculation Eq. (25).

We plot Fig. 5 in order to verify the matching degree between the time-domain signals in Fig. 4 and the theoretical normalized ACFs, Under the three turbulence states of strong, medium and weak (corresponding to Figs. 5(a)–5(c), respectively), the normalized ACFs $\psi_{\vec{I}}(\tau)$ after rank matching are well matched with the ACFs $\psi_I(\tau)$ calculated theoretically.

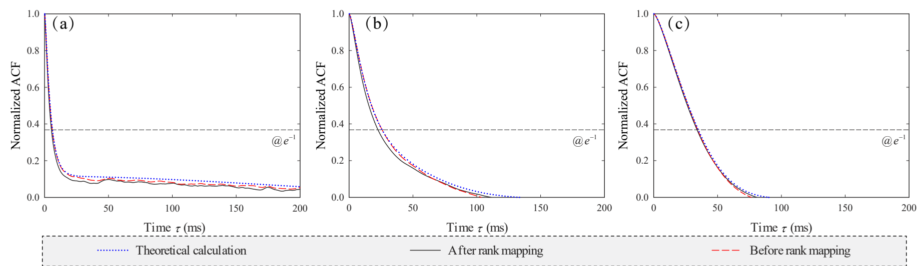

Fig. 5. ACF performance of time-domain correlated continuous sequence signals in Different turbulence fading channel. (a), (b) and (c) represent $C_n^2 = 5\times10^{-14}$ m$^{-2/3}$, $C_n^2 = 5\times10^{-15}$ m$^{-2/3}$ and $C_n^2 = 5\times10^{-16}$ m$^{-2/3}$, respectively. The light wavelength λ, and transverse wind speeds $v_\perp$ are set to $\lambda = 1550$ nm, $v_\perp = 1$ m/s and $L = 5000$ m, respectively. The blue dotted, black solid and red dashed line denote theoretical calculation I, after rank mapping $\vec{I}$ and before rank mapping $\hat{I}$, respectively.

According to Eq. (20), the correlation coefficients $\rho_{I,\vec{I}}$ between the three turbulence states can be calculated as 0.9990, 0.9993 and 0.9998 , respectively. It shows that the time-domain signals after rank matching contain strong time-domain correlation and atmospheric turbulence disturbance characteristic information. However, the statistical value of this correlation coefficient is not 1, indicating an error in the AR random process. We also draw the ACF curve $\psi_{\hat{I}}(\tau)$ of the time domain signal $\hat{I}$ before rank matching for explaining the error source. The theoretical correlation coefficients $\rho_{I,\hat{I}}$ can be calculated as 0.9992, 0.9998 and 0.9998. Obviously, $\hat{I}$ and $\vec{I}$ share the same time characteristics. The ACF $\psi_I(\tau)$ temporal information of signal I is not lost during rank matching, and it precisely inherits the ACF $\psi_{\hat{I}}(\tau)$ of $\vec{I}$, i.e., $\psi_{\vec{I}}(\tau) = \psi_{\hat{I}}(\tau) = \psi_I(\tau)$, proving that our proposed model Eq. (20) is correct.

It is worth noting that one of the key parameters used to evaluate FSOC system BER is the statistical distribution properties of time-domain light intensity signals. Therefore, the PDF cures of the time-domain continuous light intensity signal of Fig. 4 and Fig. 5 are plotted in Fig. 6. According to Eq. (20), we calculate that the correlation coefficients of Figs. 6(a)–6(c) are 0.9999, 0.9998 and 0.9999, respectively. We can deduce from Fig. 6 that the time-domain continuous light intensity signals $\vec{I}$ generated under various turbulence fading channels conform to the statistical characteristics of G-G PDFs, proving that our proposed time-domain continuous light intensity signal generation model Eq. (21) is correct.

In addition, PSD is also one of the most essential characteristics of time signals. We obtain $\vec{I}_n$, however, by ACF $\psi_I(\tau)$ Monte Carlo simulation. It's challenging to offer an analytical solution to Eq. (8) because of its intricate nature. According to the Ref. [24,33,34], we employ the weak turbulence approximation theory to simplify Eq. (8) into

$$S_I(\omega) = \frac{6.95\sigma_R^2}{\omega_\tau}\mathrm{Re}\left\{\left(\frac{\omega}{\omega_\tau}\right)^{-8/3}\left[1 - {}_1F_1\left(-\frac{5}{6};-\frac{1}{3};-\frac{i\omega^2}{2\omega_\tau^2}\right)\right]\right. \\ \left. -0.72 i^{4/3}{}_1F_1\left(\frac{1}{2};\frac{7}{3};-\frac{i\omega^2}{2\omega_\tau^2}\right)\right\}. \tag{26}$$

Equation (26) is taken logarithm, the attenuation envelope tends to a straight line with 0 slope when $\omega<\omega_t$, i.e., $\lg(S_I(\omega)) = \lg\left(6.95\sigma_R^2/\omega_\tau\right)$. Moreover, Eq. (26) can be equal to a

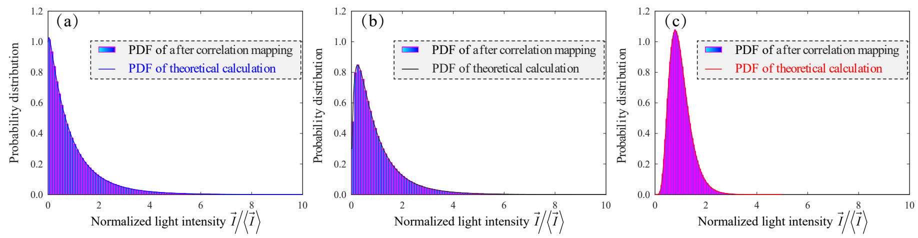

Fig. 6. PDF performances of time-domain correlated continuous sequence signals and theoretical calculations in different turbulence fading channels. (a), (b) and (c) represent $C_n^2 = 5\times10^{-14}$ m$^{-2/3}$, $C_n^2 = 5\times10^{-15}$ m$^{-2/3}$ and $C_n^2 = 5\times10^{-16}$ m$^{-2/3}$, respectively. The light wavelength λ, transverse wind speed $v_\perp$ and propagation distance L are set to $\lambda = 1550$ nm, $v_\perp = 1$ m/s and $L = 5000$ m, respectively. The blue (a), black (b) and red (c) lines represent the theoretical PDFs, respectively, and the fitting efficiencies are 0.9999, 0.9998, and 0.9999, respectively.

function with a slope of −8/3 when $\omega > \omega_t$, i.e., greater than the Fresnel frequency, indicating that the power spectrum attenuation here obeys the −8/3 rule. We have plotted theoretical fitting curves in Fig. 7(a) for turbulence intensities $C_n^2 = 5\times10^{-14}$ m$^{-2/3}$, $C_n^2 = 5\times10^{-15}$ m$^{-2/3}$ and $C_n^2 = 5\times10^{-16}$ m$^{-2/3}$, propagation distance $L = 5000$ m, and wind speed $v_\perp = 1$m/s, for example, the red, black and blue lines denote $\lg(S_I(\omega)) = -(8/3)\lg(\omega/\omega_\tau) + 5.2749$, $\lg(S_I(\omega)) = -(8/3)\lg(\omega/\omega_\tau) + 5.62749$, $\lg(S_I(\omega)) = -(8/3)\lg(\omega/\omega_\tau) + 7.2749$, respectively. The above relationships can be written as

$$\lg(S_I(\omega)) \propto \begin{cases} -\frac{8}{3}\lg\left(\frac{\omega}{\omega_\tau}\right) + \lg\left(\frac{6.95\sigma_R^2}{\omega_\tau}\right), & \omega \geq \omega_\tau \\ \lg\left(\frac{6.95\sigma_R^2}{\omega_\tau}\right), & \omega < \omega_\tau \end{cases} \tag{27}$$

where $\propto$ represents the envelope trend. We perform a fitting analysis on the PSD envelopes of the time-domain continuous light intensity signals $\vec{I}_n$ generated in Figs. 4(a)–4(c), as shown in Figs. 7(b)–7(d). The first segments of the PSD envelopes are discovered to be a comparatively smooth straight line with a slope of approximately 0 that conform to the law that the value of a straight line reduces dramatically as turbulence weakens. The curves are fitted to the second segments in Figs. 7(b)–7(d), for example blue cure $\lg\left(S_{\vec{I}}(f)\right) = -(8/3)\lg(f)$ - 0.5, black cure $\lg\left(S_{\vec{I}}(f)\right) = -(8/3)\lg(f) - 1.5$, red cure $\lg\left(S_{\vec{I}}(f)\right) = -(8/3)\lg(f) - 2.5$, which are an attenuation with a slope of −8/3 and conform to the theory shown in Eq. (27). In the comparison of Fig. 7(a), Eq. (21) highly restores the attenuation information of the atmospheric turbulence fading channel in different frequency bands. Synthesizing the information presented in Figs. 1–7, it turns out that when analyzing the FSOC performance, our proposed time-domain signal generation model may help researchers estimate the channel state information of the simulated FSOC in real-time based on the actual system and atmospheric parameters. This provides a strong theoretical basis and simulation method for signal regeneration [35], as well as being beneficial for real-time signal advanced algorithms processing [1], temporal characteristics study and adaptive optics control algorithm optimization [7], and real-time simulation of turbulent environments [20].

Optics EXPRESS

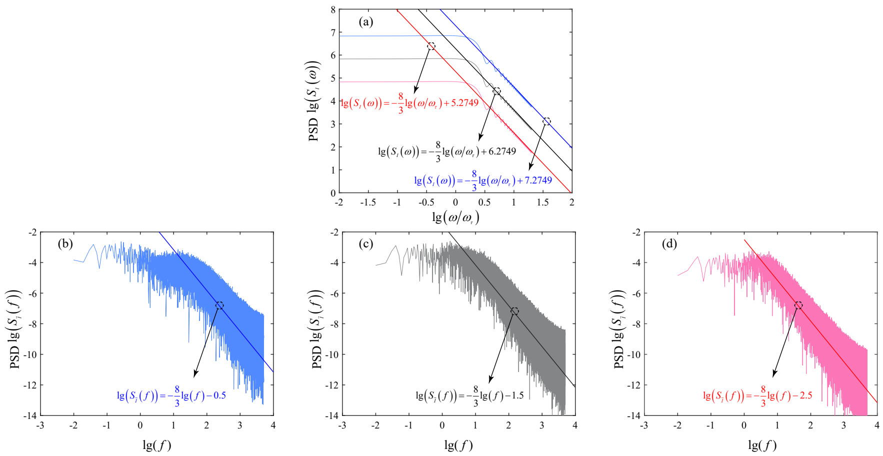

Fig. 7. Fitted PSD cure performances of time-domain correlated continuous sequence signals and theoretical calculations in different turbulence fading channels. (a) PSD curves of theoretical calculation for (b) - (d), see Eqs. (26)–(27); (b), (c) and (d) represent $C_n^2 = 5 \times 10^{-14}$ m$^{-2/3}$, $C_n^2 = 5 \times 10^{-15}$ m$^{-2/3}$ and $C_n^2 = 5 \times 10^{-16}$ m$^{-2/3}$, respectively. The light wavelength λ, transverse wind speed $v_\perp$ and propagation distance L are set to $\lambda = 1550$ nm, $v_\perp = 1$ m/s and $L = 5000$ m, respectively. The blue (a), black (b) and red (c) cures represent the fitted PSDs, respectively.

4. Conclusion

This paper proposes a continuous-time FSOC channel fading sequence generation model obeying G-G PDF, which incorporates the ACF time characteristic information of atmospheric parameters. First, the normalized channel fading function ACF model and PSD analytical formula are established under the influence of parameters such as transmission distance, optical wavelength, scintillation factor, and atmospheric structure constant. The Yule-Walker function is utilized to calculate the filter coefficients in the AR stochastic process, and the numerical solution of the time-domain Gaussian correlation sequence is derived using white Gaussian noise. Moreover, after rank mapping, a light intensity signal generation model that obeys time-domain correlation with PDF information is established, taking into account the association between the G-G parameters and the large and small scale turbulence parameters. The performances of ACF in different atmospheric conditions are then analyzed using the Monte Carlo numerical approach, and the corresponding PDFs are given. The investigations reveal that the defined Fresnel frequency ω_d may comprehensively characterize the physical meaning of ACF, and that the FSOC fading channel coherence time degradation rises as ω_d grows. We generate the sample signals of the temporal sequence under various turbulence sequences that match the waveform time characteristics reported in our previous experiments, and the scintillation indexes are highly consistent with the theoretical solution. The correlation coefficients are greater than 0.9996, and the PSDs obey the decay trend of $-8/3$ in case of various turbulence situations. The results show that the temporal sequences we generated effectively restore the fading time-domain and frequency-domain informations for the FSOC turbulence channels, providing an important theoretical basis and numerical analysis methods for the construction of real-time simulations of turbulent environments, as well as in the performances evaluation of communication BER, channel estimation, and the sample data formation of advanced modulation and demodulation algorithms.

Optics EXPRESS

Funding. Natural Science Foundation of Chongqing (cstc2021jcyj-msxmX0457); State Key Laboratory Foundation of applied optics (SKLA02022001A11); China Postdoctoral Science Foundation (2021M700415, 2021TQ0035); National Natural Science Foundation of China (61775022, 62105029, U2141231).

Disclosures. The authors declare no conflicts of interest.

Data availability. Data underlying the results presented in this paper are not publicly available at this time but may be obtained from the authors upon reasonable request.

References

1. C. Li, H. Lu, C. Chou, H. Hsia, C. Feng, Y. Chen, Y. Huang, and A. Nainggolan, "A flexible bidirectional Fiber-FSO-5G wireless convergent system," J. Lightwave Technol. **39**(5), 1296–1305 (2021).
2. M. A. Fernandes, B. T. Brandão, P. Georgieva, P. P. Monteiro, and F. P. Guiomar, "Adaptive optical beam alignment and link protection switching for 5G-over-FSO," Opt. Express **29**(13), 20136–20149 (2021).
3. V. P. Aksenov, V. V. Dudorov, V. V. Kolosov, and V. Y. Venediktov, "Probability distribution of intensity fluctuations of arbitrary-type laser beams in the turbulent atmosphere," Opt. Express **27**(17), 24705–24716 (2019).
4. H. Yao, X. Ni, C. Chen, B. Li, X. Zhang, Y. Liu, S. Tong, Z. Liu, and H. Jiang, "Performance of M-PAM FSO communication systems in atmospheric turbulence based on APD detector," Opt. Express **26**(18), 23819–23830 (2018).
5. H. Yao, X. Ni, C. Chen, B. Li, X. Feng, X. Liu, Z. Liu, S. Tong, and H. Jiang, "Performance analysis of MPSK FSOcommunication based on the balanced detector in a Fiber-Coupling system," IEEE Access **7**, 84197–84208 (2019).
6. Z. Rahman, T. Shah, S. M. Zafaruddin, and V. Chaubey, "Performance of Dual-Hop relaying for OWC system over foggy channel with pointing errors and atmospheric turbulence," IEEE Trans. Veh. Technol. **71**(4), 3776–3791 (2022).
7. H. Hemmati, *Near-earth laser communications*, vol. 143 of *Optical science and engineering* (CRC, 2009).
8. M. Tiwari, *Optical and wireless technologies: Proceedings of OWT 2020* (Springer, 2022).
9. A. Neuenkirch and L. Szpruch, "First order strong approximations of scalar SDEs defined in a domain," Numer. Math. **128**(1), 103–136 (2014).
10. V. Lyandres, "On stochastic differential equations generating non-gaussian continuous Markov process," WSEAS T. Signal Proces. **17**, 65–68 (2021).
11. J. C. Silveira Santos Filho, M. D. Yacoub, and G. Fraidenraich, "A simple accurate method for generating autocorrelated Nakagami-m envelope sequences," IEEE Commun. Lett. **11**(3), 231–233 (2007).
12. V. Lyandres, "Generating model of a sub-Rayleigh fading," J. Franklin Inst. **340**(6-7), 407–414 (2003).
13. V. M. Rennó and J. C. S. Santos Filho, "On the generation of autocorrelated $\alpha-\eta-\kappa-\mu$ fading sequences," in *2021 IEEE Statistical Signal Processing Workshop (SSP)*, (2021), pp. 291–295.
14. K. Baddour and N. Beaulieu, "Autoregressive models for fading channel simulation," in *IEEE Global Telecommunications Conference*, vol. 2 (2001), pp. 1187–1192.
15. R. B. Ertel and J. H. Reed, "Generation of two equal power correlated Rayleigh fading envelopes," IEEE Commun. Lett. **2**(10), 276–278 (1998).
16. H. T. Yura and S. G. Hanson, "Digital simulation of an arbitrary stationary stochastic process by spectral representation," J. Opt. Soc. Am. A **28**(4), 675–685 (2011).
17. B. Epple, "Simplified channel model for simulation of Free-Space optical communications," J. Opt. Commun. Netw. **2**(5), 293 (2010).
18. K. E. Baddour and N. C. Beaulieu, "Autoregressive modeling for fading channel simulation," IEEE T. Wirel. Commun. **4**(4), 1650–1662 (2005).
19. D. Bykhovsky, "Simple generation of Gamma, Gamma–Gamma, and K distributions with exponential autocorrelation function," J. Lightwave Technol. **34**(9), 2106–2110 (2016).
20. D. Bykhovsky, "Free-space optical channel simulator for weak-turbulence conditions," Appl. Opt. **54**(31), 9055–9059 (2015).
21. A. Jurado-Navas, A. García-Zambrana, and A. Puerta-Notario, "Efficient lognormal channel model for turbulent FSO communications," Electron. Lett. **43**(3), 178 (2007).
22. A. Jurado-Navas and A. Puerta-Notario, "Generation of correlated scintillations on atmospheric optical communications," J. Opt. Commun. Netw. **1**(5), 452 (2009).
23. H. Yao, C. Chen, X. Ni, S. Tong, B. Li, P. Chidike, Z. Liu, Y. Zhao, and H. Jiang, "Analysis and evaluation of the performance between reciprocity and time delay in the atmospheric turbulence channel," Opt. Express **27**(18), 25000–25011 (2019).
24. L. C. Andrews and R. L. Phillips, *Laser beam propagation through random media* (SPIE, 2005), 2nd ed.
25. L. C. Andrews, R. L. Phillips, C. Y. Hopen, and M. A. Al-Habash, "Theory of optical scintillation," J. Opt. Soc. Am. A **16**(6), 1417 (1999).
26. D. G. Manolakis, V. K. Ingle, and S. M. Kogon, *Statistical and adaptive signal processing: Spectral estimation, signal modeling, adaptive filtering, and array processing*, Artech House signal processing library (Artech House, 2005).
27. P. Stoica and R. L. Moses, *Spectral analysis of signals* (Pearson Prentice Hall, 2005).

Optics EXPRESS

28. A. G. Marques, S. Segarra, G. Leus, and A. Ribeiro, "Stationary graph processes and spectral estimation," IEEE T. Signal Proces. **65**(22), 5911–5926 (2017).
29. J. Cadzow, "High performance spectral estimation–a new ARMA method," IEEE Trans. Acoust., Speech, Signal Process. **28**(5), 524–529 (1980).
30. B. Friedlander and B. Porat, "The modified Yule-Walker method of ARMA spectral estimation," IEEE Trans. Aerosp. Electron. Syst. **AES-20**(2), 158–173 (1984).
31. H. Lim and D. Yoon, "Generalized moment-based estimation of Gamma-Gamma fading channel parameters," IEEE Trans. Veh. Technol. **67**(1), 809–811 (2018).
32. A. Kellerer and A. Tokovinin, "Atmospheric coherence times in interferometry: definition and measurement," Astron. Astrophys. **461**(2), 775–781 (2007).
33. W. Du, L. Tan, J. Ma, and Y. Jiang, "Temporal-frequency spectra for optical wave propagating through non-Kolmogorov turbulence," Opt. Express **18**(6), 5763–5775 (2010).
34. L. Cui, "Analysis of temporal power spectra for optical waves propagating through weak anisotropic non-Kolmogorov turbulence," J. Opt. Soc. Am. A **32**(6), 1199–1208 (2015).
35. M. A. Amirabadi, M. H. Kahaei, S. A. Nezamalhosseini, and V. T. Vakili, "Deep learning for channel estimation in FSO communication system," Opt. Commun. **459**, 124989 (2020).